ARTICLE IN PRESS

Available online at www.sciencedirect.com
SCIENCE DIRECT®

Pattern Recognition Letters xxx (2005) xxx–xxx

Pattern Recognition Letters

www.elsevier.com/locate/patrec

Astronomical image restoration using an improved anisotropic diffusion

Shin-Min Chao, Du-Ming Tsai *

Department of Industrial Engineering and Management, Yuan-Ze University, 135 Yuan-Tung Road, Nei-Li, Tao-Yuan 32026, Taiwan, ROC

Received 1 November 2004; received in revised form 22 July 2005

Communicated by T.K. Ho

Abstract

Images secured from an astronomical telescope usually suffer from blur and from interference that scientists refer to as "noise". Therefore, good image restoration technique has become an important tool in astronomical observation. In this paper, we propose a modified anisotropic diffusion scheme to tackle the problem of image restoration in astronomy, especially in the case of nebula images. In such images, a mass of stars may be extremely bright but also may be spread randomly in dark space, and the shape of the nebula may therefore appear obscure. To restore the original appearance of a nebula, noisy stars must be filtered out and the detailed structure of the nebula must be well enhanced. The classical Perona–Malik anisotropic diffusion model that only considers gradient information cannot filter out noisy stars from the nebula image. In this study, we propose a modified anisotropic diffusion model that incorporates both gradient and gray-level variance information to remove "sparking" stars of various sizes and brightness in a nebula image. Experimental results from a number of astronomical nebula images have shown that the proposed anisotropic diffusion scheme can effectively remove noisy stars and maintain the shape of nebula in this particular case.

Keywords: Astronomical image restoration; Nebula image; Anisotropic diffusion

1. Introduction

The field of image restoration has a long history that began in the 1950s with the space program. The objective of image restoration is to reconstruct the original image from its degraded version. The image restoration techniques are widely used in various applications such as satellite imaging (Jalobeanu et al., 2000; Bretschneider, 2002; Bratsolis and Sigelle, 2003), medical imaging (Rathee et al., 1992; Lee et al., 2004), astronomical imaging (Molina, 1994; Molina et al., 2001), forensic science (Wen and Lee, 2002) and many other poor-quality imaging. In this paper, we especially focus on the problem of image restoration in astronomy.

There are a few problems regarding the image secured from an astronomical telescope, such as blur and noise. The objectives of image restoration techniques for astronomy roughly include de-blurring, removal of atmospheric visibility degradation, correction of mirror spherical aberration, image sharpening, image zooming, and optimizing display (Starck et al., 2002). Much research has been done on the field of image restoration in astronomy. Molina et al. (2001) proposed Bayesian image restoration methods and used expectation-maximization (EM) algorithms to restore noise and blur in astronomical images. Starck et al. (2003) combined both the wavelet and two newly multiscale approaches of ridgelet and curvelet transforms, to the problem of restoring an astronomical image from noisy data. Due to the high-directional sensitivity of the two multiscale representations, their method can well enhance elongated features contained in the astronomical images. Wu and Barba (1998) proposed an algorithm for the restoration of star field images by incorporating both the

* Corresponding author. Tel.: +886 3 463 8800; fax: +886 3 463 8907.
E-mail address: iedmtsai@saturn.yzu.edu.tw (D.-M. Tsai).

0167-8655/$ - see front matter © 2005 Elsevier B.V. All rights reserved.
doi:10.1016/j.patrec.2005.08.021

minimum mean square error criteria and the maximum varimax criteria.

The traditional image restoration techniques for astronomy mainly focus on de-blurring and noise removal. In order to restore the object effectively, most of the methods use the point spread function (PSF) to de-blend images. These methods assume that the PSF in an image has been known or can be estimated based on a priori knowledge. However, the PSF and useful prior knowledge are not always available in most practical situations. There are other common denoising methods such as Bayesian estimate, maximum likelihood (ML) and maximum a posteriori (MAP) to estimate an original clean image from a corrupted image that contains Gaussian noise (Mihcak et al., 1999; Moulin and Liu, 1999; Nikolova, 1999; Dias and Leitao, 2002; Deng, 2004). The main difficulties in MAP estimation are the choices of a proper prior distribution of the estimated image, and the corresponding energy function to be optimized.

In this paper, we propose an anisotropic diffusion scheme to tackle the problem of image restoration in astronomy, especially the nebula images. In a nebula image, a mass of stars are bright and spread randomly in the dark space, and the shape of the nebula is obscure. It is not easy for the astronomers to observe the nebula's outline. Fig. 1 shows an example of the Henize 70 nebula image obscured with sparking stars. For the analysis of nebulae in astronomical images, we must eliminate the small bright points in the dark background. The proposed diffusion model will effectively remove sparking stars and enhance the nebula shapes without the intervention of human experts. It does not need to estimate the PSF and MAP from astronomical images.

The anisotropic diffusion was first proposed by Perona and Malik (1990) for scale-space description of images and edge detection. This approach is basically a modification of the linear diffusion (or heat equation), and the continuous anisotropic diffusion is given by

$$\frac{\partial \boldsymbol{I}_t(x,y)}{\partial t} = \operatorname{div}\left[\boldsymbol{c}_t \cdot \nabla \boldsymbol{I}_t(x,y)\right] \tag{1}$$

where $\boldsymbol{I}_t(x,y)$ is the image at time t; div represents the divergence operator; $\nabla \boldsymbol{I}_t(x,y)$ is the gradient of the image, and $\boldsymbol{c}_t$ represents the diffusion coefficient. Eq. (1) will reduce to an isotropic diffusion equation if the diffusion coefficient $\boldsymbol{c}_t$ is a constant. It is then equivalent to convolving the image with a Gaussian filter. The idea of anisotropic diffusion is to adaptively choose $\boldsymbol{c}_t$ in different iterations so that intra-regions in an image become smooth while edges of inter-regions are sharply preserved. The diffusion coefficient $\boldsymbol{c}_t$ is generally selected to be a nonnegative monotonically decreasing function of gradient magnitude so that small variations of intensity such as noise or shading can be well smoothed, while edges with large intensity transition are distinctly retained.

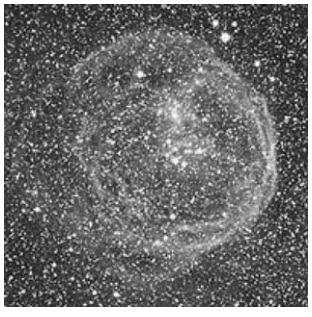

Fig. 1. The Henize 70 nebula obscured by sparking stars (original image courtesy of Anglo–Australian Observatory).

Hamza et al. (2002) described that the MAP estimator for a noiseless image u can be given by

$$\hat{u} = \arg\min_{u}\left\{F(u) + \frac{\lambda}{2}|u-u_0|^2\right\}$$

where $\hat{u}$ is an estimate for u; u_0 is the observed image; λ is a constant, and F is a given energy function. You et al. (1996) considered the anisotropic diffusion as the gradient descent method for solving an energy minimization problem. They also showed that the Perona–Malik diffusion in Eq. (1) is the gradient descent flow for a properly selected energy function $F(u)$.

Barash (2002) addressed the fundamental relationship between anisotropic diffusion and adaptive smoothing. He showed that an iteration of adaptive smoothing

$$\boldsymbol{I}_{t+1}(x,y) = \frac{\sum_i \sum_j \boldsymbol{I}_t(x+i,y+j) w_t(x+i,y+j)}{\sum_i \sum_j w_t(x+i,y+j)} \tag{2}$$

is an implementation of the discrete version of the anisotropic diffusion equation if the weight w_t in Eq. (2) is taken as the same of the diffusion coefficient $\boldsymbol{c}_t$ in Eq. (1). The anisotropic diffusion approach has become an useful tool for edge detection (Alvarez et al., 1992; Chen and Barcelos, 2001), image enhancement (Sapiro and Ringach, 1996; Solé and López, 2001), image smoothing (Torkamani-Azar and Tait, 1996; Tsuji et al., 2002), image segmentation (Niessen et al., 1997; Bakalexis et al., 2002), texture segmentation (Deng and Liu, 2000), defect detection (Tsai and Chao, 2005) and image restoration (You and Kaveh, 1999). However, the anisotropic diffusion approach has not been used in image restoration in astronomy. In order to restore the nebula outline obscured by sparking stars, the stars should be filtered out from the astronomical image. The classical anisotropic diffusion model of Perona and Malik (P–M model) only considers the gradient information of the image. When using the P–M model to restore a astronomical nebula image, the bright stars in a dark background will result in large magnitude of gradient, and cannot be filtered out successfully. In this study, the gray-level variance information along with the gradient is added to a modified anisotropic model for image restoration. The proposed method can effectively remove the tiny sparking stars and enhance the shape of nebula in the restored image.

The organization of this paper is as follows: Section 2 first overviews the anisotropic diffusion equation of Perona and Malik. The proposed anisotropic diffusion scheme that adaptively smoothes or retains gray levels by taking into account both gray-level variance and gradient for astronomical image restoration is then discussed. Section 3 presents experimental results from a number of astronomical nebula images. This paper is concluded in Section 4.

2. The modified anisotropic diffusion model

2.1. The Perona–Malik anisotropic diffusion

Let $\boldsymbol{I}_t(x,y)$ be the gray level at coordinates (x,y) of a digital image at iteration t, and $\boldsymbol{I}_0(x,y)$ the original input image. The continuous anisotropic diffusion in Eq. (1) can be discretely implemented by using four nearest neighbors and the Laplacian operator (Perona and Malik, 1990)

$$\boldsymbol{I}_{t+1}(x,y) = \boldsymbol{I}_t(x,y) + \frac{1}{4}\sum_{i=1}^{4}[\boldsymbol{c}_t^i(x,y)\cdot\nabla\boldsymbol{I}_t^i(x,y)]$$

where $\nabla\boldsymbol{I}_t^i(x,y)$, $i=1$, 2, 3 and 4, represent the gradients of four neighbors in the north, south, east and west directions, respectively, i.e.,

$$\nabla\boldsymbol{I}_t^1(x,y) = \boldsymbol{I}_t(x,y-1) - \boldsymbol{I}_t(x,y)$$
$$\nabla\boldsymbol{I}_t^2(x,y) = \boldsymbol{I}_t(x,y+1) - \boldsymbol{I}_t(x,y)$$
$$\nabla\boldsymbol{I}_t^3(x,y) = \boldsymbol{I}_t(x+1,y) - \boldsymbol{I}_t(x,y)$$
$$\nabla\boldsymbol{I}_t^4(x,y) = \boldsymbol{I}_t(x-1,y) - \boldsymbol{I}_t(x,y)$$

$\boldsymbol{c}_t^i(x,y)$ is the diffusion coefficient associated with $\nabla\boldsymbol{I}_t^i(x,y)$, and is considered as a function of the gradient $\nabla\boldsymbol{I}_t^i(x,y)$ in the P–M model, i.e.,

$$\boldsymbol{c}_t^i(x,y) = g(\nabla\boldsymbol{I}_t^i(x,y))$$

For the sake of simplicity, $\nabla\boldsymbol{I}_t^i(x,y)$ is subsequently denoted by $\nabla\boldsymbol{I}$. The function $g(\nabla\boldsymbol{I})$ has to be a nonnegative monotonically decreasing function with $g(0)=1$ and $\lim_{|\nabla\boldsymbol{I}|\to\infty} g(\nabla\boldsymbol{I}) = 0$. The function $g(\nabla\boldsymbol{I})$ should result in low coefficient values at image edges that have large gradients, and high coefficient values within image regions that have low gradients. In the Perona–Malik anisotropic diffusion model, a possible diffusion coefficient function is given by

$$g(\nabla\boldsymbol{I}) = 1/[1+(|\nabla\boldsymbol{I}|/\mathscr{K})^2] \tag{3}$$

where the parameter $\mathscr{K}$ is a constant, and must be fine-tuned for a particular application. Parameter $\mathscr{K}$ in the diffusion coefficient function acts as an edge strength threshold. If the $\mathscr{K}$ value is too large, the diffusion process will oversmooth and result in a blurred image. In contrast, if the $\mathscr{K}$ value is too small, the diffusion process will stop the smoothing in early iterations and yield a restored image similar to the original one.

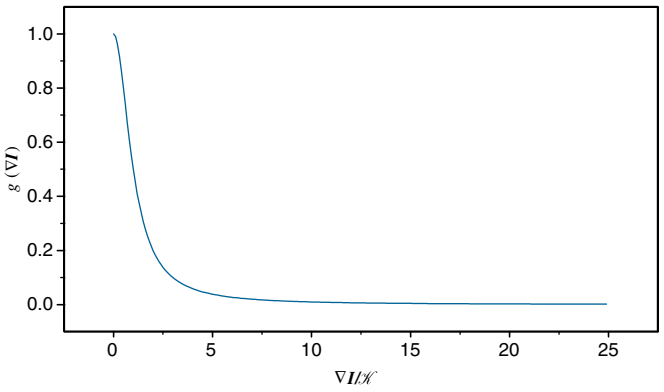

Fig. 2. Graph of the diffusion coefficient function: $g(\nabla\boldsymbol{I}) = 1/[1+(|\nabla\boldsymbol{I}|/\mathscr{K})^2]$.

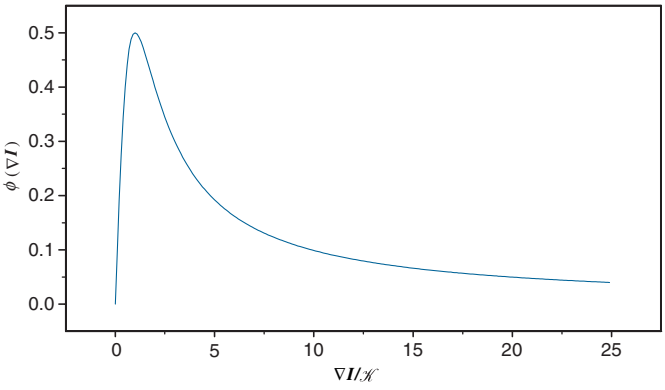

Fig. 3. Graph of the flux function: $\phi(\nabla\boldsymbol{I}) = \{1/[1+(|\nabla\boldsymbol{I}|/\mathscr{K})^2]\}\cdot\nabla\boldsymbol{I}$.

Let $\phi(\nabla\boldsymbol{I})$ be a flux function (Perona and Malik, 1990) defined by

$$\phi(\nabla\boldsymbol{I}) = g(\nabla\boldsymbol{I})\cdot\nabla\boldsymbol{I} \tag{4}$$

A large flux value indicates a strong effect on smoothness. Figs. 2 and 3 depict the diffusion coefficient function and the flux function in Eqs. (3) and (4), respectively. For a given $\mathscr{K}$ value, it can be seen from Fig. 2 that the diffusion coefficient function in Eq. (3) drops dramatically and approximates to zero when the gradient magnitude $|\nabla\boldsymbol{I}|$ is larger than $5\mathscr{K}$. That is, the diffusion stops as soon as $|\nabla\boldsymbol{I}| > 5\mathscr{K}$. The maximum smoothness occurs at $|\nabla\boldsymbol{I}| = 1\mathscr{K}$, as shown in the corresponding flux function. The classical P–M model considers only the gradient information of image for image restoration. Therefore, it cannot effectively eliminate noises with large gradient or preserve target objects with low gradient in an ill-structured image.

2.2. The proposed anisotropic diffusion

In this study, our objective is to restore the unclear shape of a nebula obscured by sparking stars in an astronomical image. Observing the previous nebula image in Fig. 1, we find numerous bright stars spread randomly all over the image. Those tiny bright stars have very high gray values. They may embedded in the dark background of low

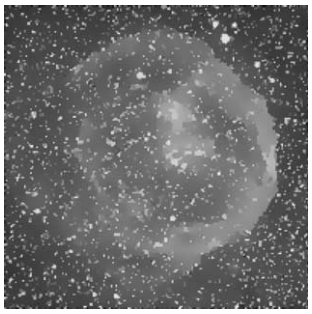

Fig. 4. The result of the traditional P–M diffusion for the nebula image in Fig. 1 (after 50 iterations and $\mathscr{K} = 8$).

gray values, or in front of the nebula region of high gray values. It indicates that the traditional P–M model that only takes into account the gradient information cannot sufficiently remove the stars even after a long sequence of iterations. Fig. 4 shows the result after 50 iterations of the diffusing process using the P–M model with a properly selected parameter value $\mathscr{K} = 8$. It can be found from the figure that the stars are still retained, but the details of the nebula have been destroyed in the restored image. It is not an acceptable result for astronomers to distinguish the complexion of the nebula.

Since the stars have bright intensities and scatter in the dark space in a nebula image, it infers that there are larger variances of gray levels in the neighborhood of stars, compared with those of the nebula. In order to remove sparking stars effectively in a nebula image, we incorporate the local variance information of gray levels in the diffusion model. By including the gray-level variance in the diffusion process, the diffusion coefficient function in Eq. (3) is revised as

$$g(\nabla \boldsymbol{I}, \sigma^2) = 1 \Big/ \left[1 + \left(\frac{|\nabla \boldsymbol{I}|}{\mathscr{K}_0 \cdot \sigma^2}\right)^2\right] \tag{5}$$

where $\mathscr{K}_0$ is a positive constant, and σ^2 is the local variance of gray levels in a 3×3 neighborhood window. For a given pixel of coordinates (x, y) at iteration t, the variance is defined by

$$\sigma_t^2(x,y) = \frac{1}{9}\sum_{i=-1}^{1}\sum_{j=-1}^{1}(\boldsymbol{I}_t(x+i, y+j) - \overline{\boldsymbol{I}}_t(x,y))^2$$

where $\overline{\boldsymbol{I}}_t(x,y)$ is the mean of gray levels in the 3×3 neighborhood window. If σ^2 is fixed throughout the entire image, $\mathscr{K}_0 \cdot \sigma^2$ will become a constant and the modified diffusion model with the diffusion coefficient function in Eq. (5) will be equivalent to the P–M model. The modified diffusion coefficient function in Eq. (5) is a function of two variables, the gradient $\nabla \boldsymbol{I}$ and the gray-level variance σ^2. The new flux function is given by

$$\phi(\nabla \boldsymbol{I}, \sigma^2) = g(\nabla \boldsymbol{I}, \sigma^2) \cdot \nabla \boldsymbol{I} \tag{6}$$

In a nebula image, noisy stars are bright and spread randomly in the dark space. With such characteristics, stars have both a large gradient value $\nabla \boldsymbol{I}$ and a large variance value σ^2, and σ^2 is more significant than $\nabla \boldsymbol{I}$ in terms of magnitudes. However, the gray levels of a nebula are changed gradually in the dark space. In the nebula regions, the gray-level variance σ^2 is relatively small, and is not as significant as the gradient magnitude $\nabla \boldsymbol{I}$. Fig. 5 presents the 3D curved surface of the diffusion coefficient function in Eq. (5) as functions of $\nabla \boldsymbol{I}/\mathscr{K}_0$ and σ^2. When the gradient magnitude $\nabla \boldsymbol{I}$ increases, the value of the diffusion coefficient function is reduced gradually as occurs in the traditional P–M model does. However, when σ^2 is significantly larger than $\nabla \boldsymbol{I}/\mathscr{K}_0$, the function value will dramatically increase to one and results in a strong smoothing in the diffusion process. Therefore, the stars can be effectively filtered out in the restored image. When $\nabla \boldsymbol{I}/\mathscr{K}_0$ is reversely larger than σ^2, the value of the diffusion coefficient function will be close to zero and the smoothing operation will not be carried out in the diffusion process. Therefore, the shape of nebula can be completely preserved in the restored image. Fig. 6 illustrates the 3D curved surface of the flux function in Eq. (6). It represents the degree of diffusion effect as a function of $\nabla \boldsymbol{I}/\mathscr{K}_0$ and σ^2. When both $\nabla \boldsymbol{I}$ and σ^2 increase simultaneously, the value of flux function will dramatically increase. That is, the high variance and high gradient strengthen the diffusion process

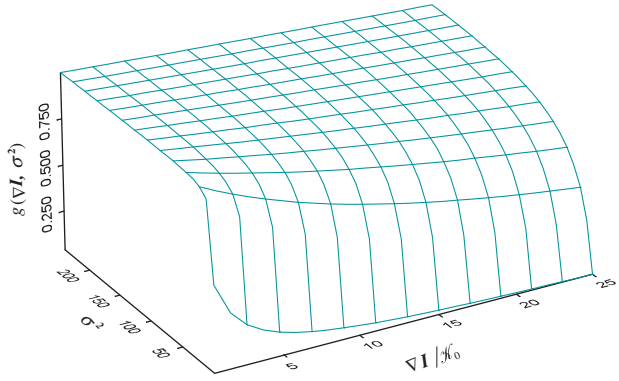

Fig. 5. Graph of the diffusion coefficient function $g(\nabla \boldsymbol{I}, \sigma^2) = 1 \Big/ \left[1 + \left(\frac{|\nabla \boldsymbol{I}|}{\mathscr{K}_0 \cdot \sigma^2}\right)^2\right]$ with two variables of $\nabla \boldsymbol{I}/\mathscr{K}_0$ and σ^2.

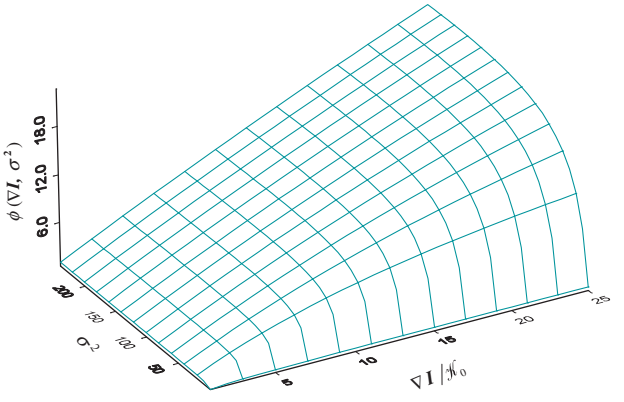

Fig. 6. Graph of the new flux function $\phi(\nabla \boldsymbol{I}, \sigma^2)$ containing both gradient and gray-level variance variables.

since a large flux value indicates a strong effect on smoothness. In a nebula image, the bright stars have higher variance and higher gradient than those of the nebula. The noisy stars can be effectively eliminated and the shape of nebula can be well enhanced by incorporating both gray-level variance and gradient in the diffusion model.

In the P–M model, the degree of diffusion is based on the gradient value with respect to a constant parameter $\mathcal{K}$, as seen in Eq. (3). In the P–M model, the value of parameter $\mathcal{K}$ is fixed throughout the entire image in every iteration. We can describe the modified diffusion model that involves two variables of gradient and local variance from the aspect of adaptive $\mathcal{K}$. In the proposed diffusion coefficient function of Eq. (5), $\mathcal{K}_0 \cdot \sigma^2$ can be considered as an adaptive version of $\mathcal{K}$ in the P–M model (Eq. (3)). Each individual pixel in the modified diffusion model has its own $\mathcal{K}$ value, which is determined by the magnitude of its local variation. The adaptive $\mathcal{K}$ function for a pixel at coordinates (x, y) is defined by

$$\mathcal{K}(x, y) = \mathcal{K}_0 \cdot \sigma^2(x, y) \tag{7}$$

where $\sigma^2(x, y)$ is the variance defined in a small neighborhood of (x, y). $\mathcal{K}(x, y)$ is proportional to the variance $\sigma^2(x, y)$. When $\mathcal{K}(x, y)$ is significantly larger than the gradi-

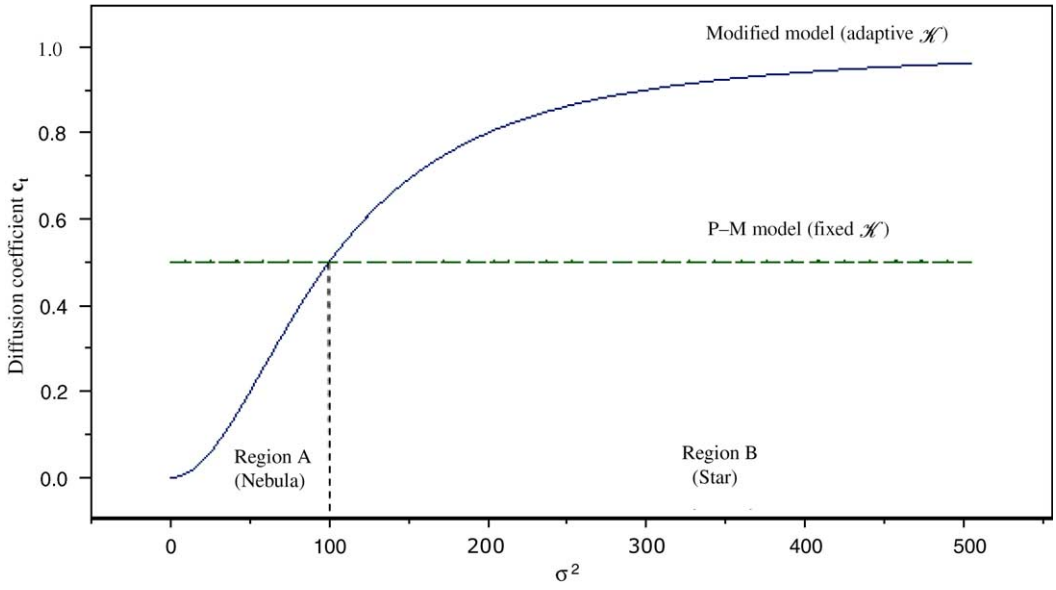

Fig. 7. Diffusion coefficients c_t for the P–M model and the modified diffusion model under a given gradient value ∇I.

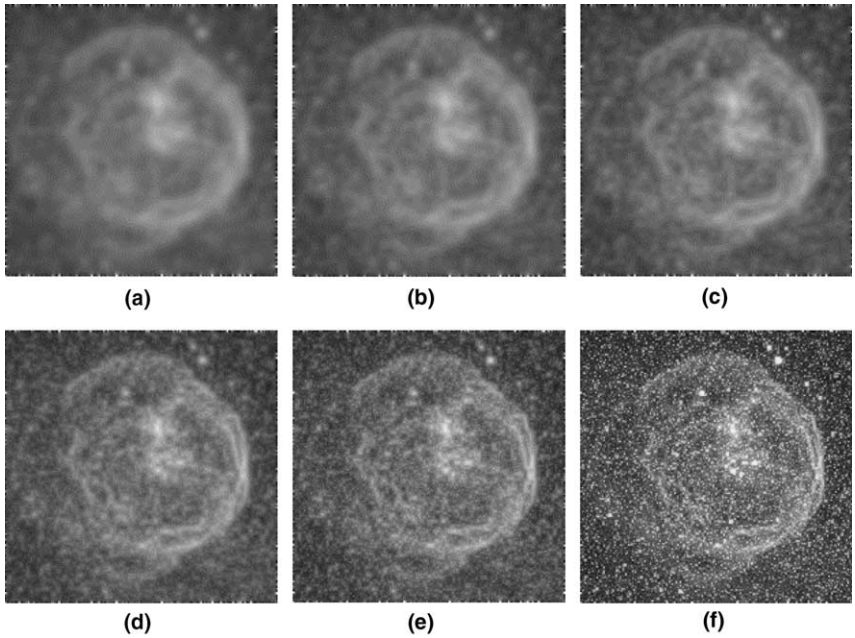

Fig. 8. The restored results of the nebula image in Fig. 1 from various values of $\mathcal{K}_0$: (a)–(f) the restored images from $\mathcal{K}_0 = 5$, 1, 0.5, 0.1, 0.05 and 0.01, respectively.

ent $\nabla \boldsymbol{I}$, the value of diffusion coefficient function will also be large and the modified model gives a strong smoothing. A noisy star has a large variance and, therefore, it results in a large $\mathscr{K}$ value for strong smoothing. When $\nabla \boldsymbol{I}$ is reversely larger than $\mathscr{K}(x, y)$, the function value will be small and the modified diffusion model stops the smoothing. This prevents the blurring of nebular edges.

Fig. 7 shows the curves of diffusion coefficients for the P–M model and the modified diffusion model under a given $\nabla \boldsymbol{I}$. For a given value of $\nabla \boldsymbol{I}$, the diffusion coefficient $\boldsymbol{c}_t$ of the P–M model will be the same since a constant $\mathscr{K}$ is used. However, the value of $\boldsymbol{c}_t$ in the modified diffusion model will vary according to the local variance since the parameter $\mathscr{K}$ is adaptively determined by $\mathscr{K}_0 \cdot \sigma^2$. The value of $\boldsymbol{c}_t$ increases as the value of σ^2 increases. In our study, it can be inferred that the variance of a nebula area may locate in region A in Fig. 7 because the gray levels around the nebula are changed gradually and smoothly. Conversely, the variance of noisy stars may locate in region B in Fig. 7 because the stars have bright intensities in the dark background. The P–M model cannot find a suitably fixed value for the parameter $\mathscr{K}$ that can simultaneously remove noisy stars and preserve the shape of a nebula in an image. A small fixed $\mathscr{K}$ value disables the diffusion process and cannot remove the noisy stars effectively. A large $\mathscr{K}$ fixed value will oversmooth both nebula and stars. In a nebula area (region A), the modified diffusion model with a small adaptive $\mathscr{K}$ provides little smoothing effect and preserves the details of the nebula. In a noisy star area (region B), the modified diffusion model with a large adaptive $\mathscr{K}$ yields a stronger smoothing effect and well eliminates the noisy stars. The adaptive parameter $\mathscr{K}$ allows the modified diffusion model to eliminate noisy stars and retain a nebular shape at the same time without conflict.

Since the parameter $\mathscr{K}_0$ must be fine-tuned for a particular application, the following experiments are performed to find out the suitable value of $\mathscr{K}_0$ for the restoration of nebula images. Fig. 8(a)–(f) shows the restored results of the sample image in Fig. 1 for various values of $\mathscr{K}_0 = 5$, 1, 0.5, 0.1, 0.05 and 0.01, respectively. The number of iterations is set to 10 for all tests. When $\mathscr{K}_0$ is overly large, the resulting images are severely blurred. Not only the stars are totally filtered out, but also the detailed features of the nebula is lost, as seen in Fig. 8(a)–(c). In contrast, when $\mathscr{K}_0$ is overly small, the restored result in Fig. 8(f) shows that the diffusion process cannot effectively remove the noisy stars and the filtered image is similar to the original one. Fig. 8(d) and (e) both have a good effect on eliminating

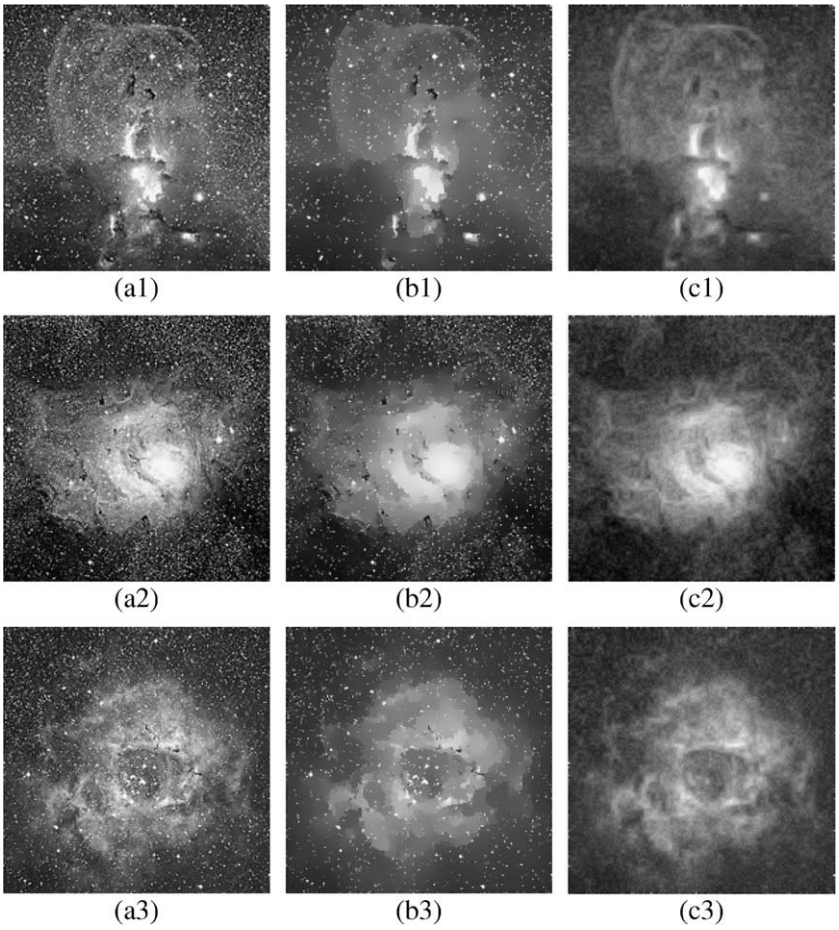

Fig. 9. (a1)–(a3) three original nebula images of NGC 3576, NGC 6523 and NCG 2244, respectively; (b1)–(b3) the restoration results of the traditional P–M diffusion model; (c1)–(c3) the results of the proposed diffusion model (original images courtesy of Anglo–Australian Observatory).

the noisy stars. The shape of nebula restored in Fig. 8(e) is clearer than the one shown in Fig. 8(d). By considering the effective removal of noisy stars and preservation of nebula details in the restored image, the suitable value of $\mathscr{K}_0$ in Eq. (5) is 0.05 for the application of nebula image restoration. Note that the value of $\mathscr{K}_0$ in Eq. (5) depends on the intensity range of the input image.

3. Experimental results

In this section, we present experimental results from a number of astronomical nebula images. All the nebula images for testing were obtained from the Anglo–Australian Observatory (http://www.aao.gov.au/). The algorithms were implemented on a Pentium 4, 3 GHz personal computer using the Visual Basic language. The images were 200×200 pixels wide with 8-bit gray levels. The value of parameter $\mathscr{K}_0$ in the diffusion coefficient function of Eq. (5) was set to a fixed value of 0.05, and the number of iterations equals to 10 for all test images in the following experiments. Computation time of 10 iterations on a 200×200 image was 0.2 s.

The test images in Fig. 9(a1)–(a3) presents three types of nebula images obscured with sparking stars. The restoration results from the traditional P–M diffusion model that considers only the gradient information are shown in Fig. 9(b1)–(b3). It can be found from the figure that the bright stars cannot be removed effectively and the detailed structures of the nebulae are destroyed. Fig. 9(c1)–(c3) show the restored results from the proposed diffusion model that takes into account both gradient and gray-level variance. From the figure, it appears that the noisy stars are effectively filtered out and the original appearance of the nebula is very well preserved.

Fig. 10(a1)–(a3) presents three additional nebula images that contain more noisy stars and make the nebulae hardly visible. The structures and appearances of these three nebula images are more obscure, compared with those in Fig. 9. Fig. 10(b1)–(b3) show the results from the traditional P–M diffusion model. As with those shown in Fig. 9(b1)–(b3), the restored images are not satisfactory with the P–M model. Fig. 10(c1)–(c3) presents the restored images from the proposed diffusion model. It can be found that the proposed method can reliably eliminate all sizes of

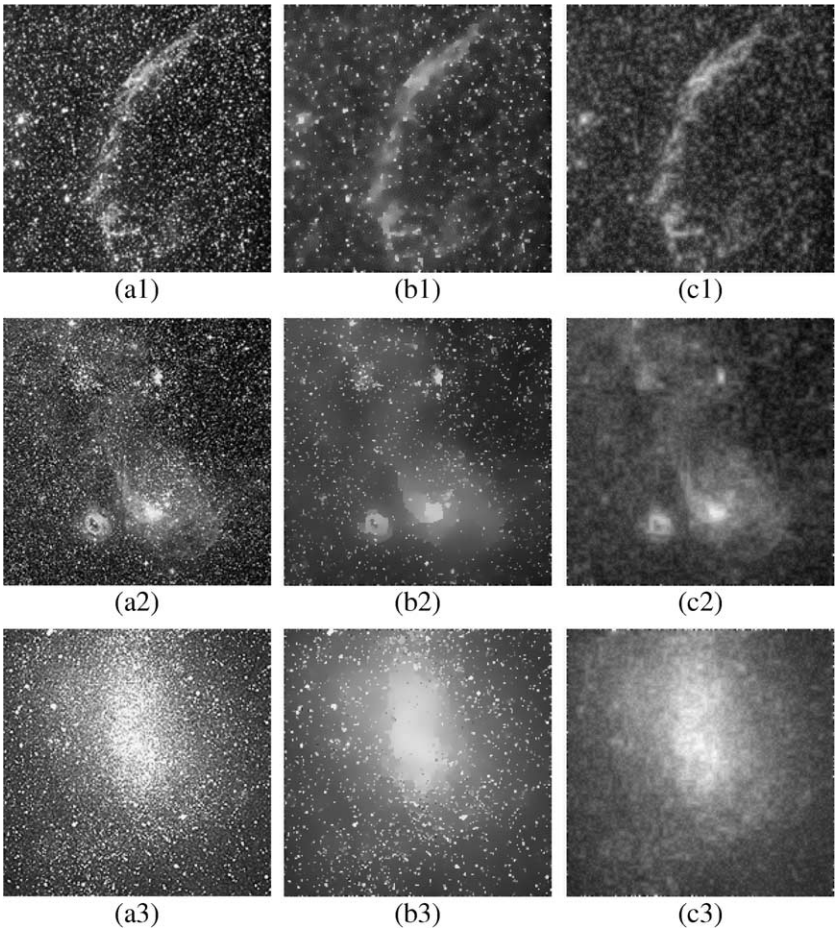

Fig. 10. Three sample images that contain more noisy stars: (a1)–(a3) original nebula images of NGC 6995, NGC 2014 and NCG 6822, respectively; (b1)–(b3) the restoration results of the traditional P–M diffusion model; (c1)–(c3) the results of the proposed diffusion model (original images courtesy of Anglo–Australian Observatory).

bright stars and keep the shape of the nebula visible to observers.

In order to further verify the performance of the proposed method, the commonly denoising techniques including Gaussian smoothing, median filtering and Fourier transform were used for comparison. Figs. 11(a)–14(a) show the restored results from the proposed method that incorporates both gradient and local variance information, and Figs. 11(b)–14(b) present the restored images by using the Gaussian smoothing, in which the noisy stars cannot be sufficiently removed. Figs. 11(c)–14(c) show the restored images from the median filter. It can be observed that some smaller stars can be eliminated, but larger bright stars still remain in the filtered images. The Fourier transform blurs the whole image including the nebula and stars, as seen in Figs. 11(d)–14(d).

In the experiments, two locally adaptive denoising algorithms that use local variances to estimate the desired intensities in the original image are also evaluated. The two adaptive denoising methods selected are the Wiener fil-

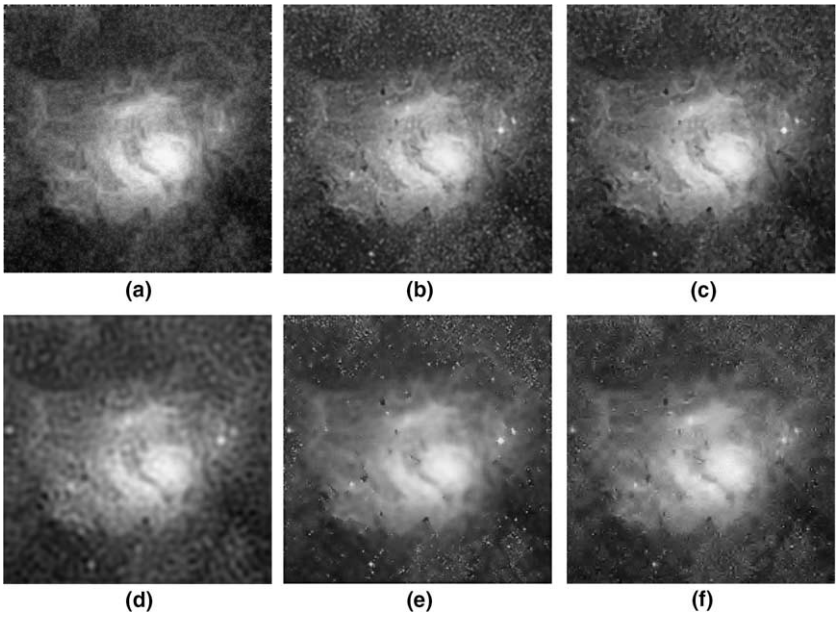

Fig. 11. Comparison of the restoration results in Fig. 9(a2) from various filtering methods: (a) the proposed diffusion model; (b) Gaussian smoothing; (c) median filter; (d) Fourier transform; (e) Wiener filtering; (f) wavelet shrinkage.

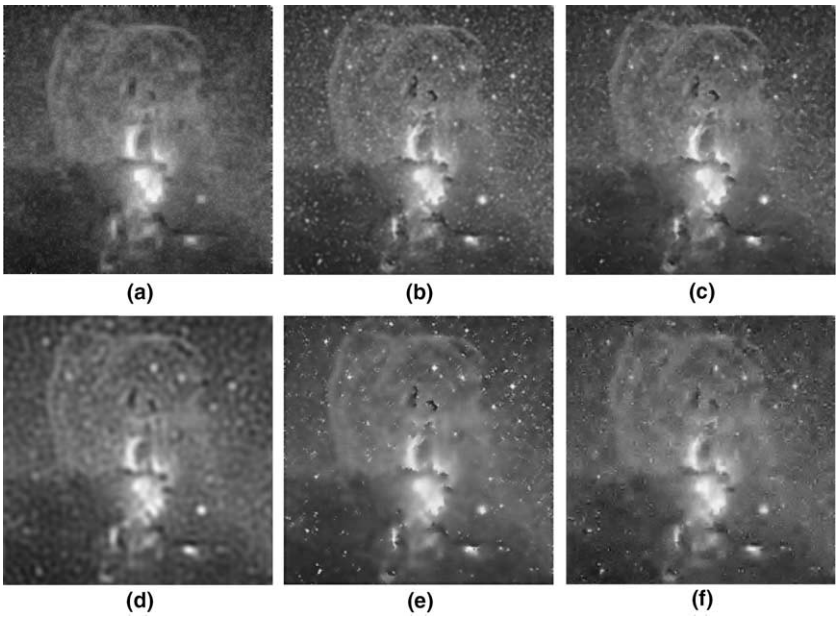

Fig. 12. Comparison of the restoration results in Fig. 9(a1) from various filtering methods: (a) the proposed diffusion model; (b) Gaussian smoothing; (c) median filter; (d) Fourier transform; (e) Wiener filtering; (f) wavelet shrinkage.

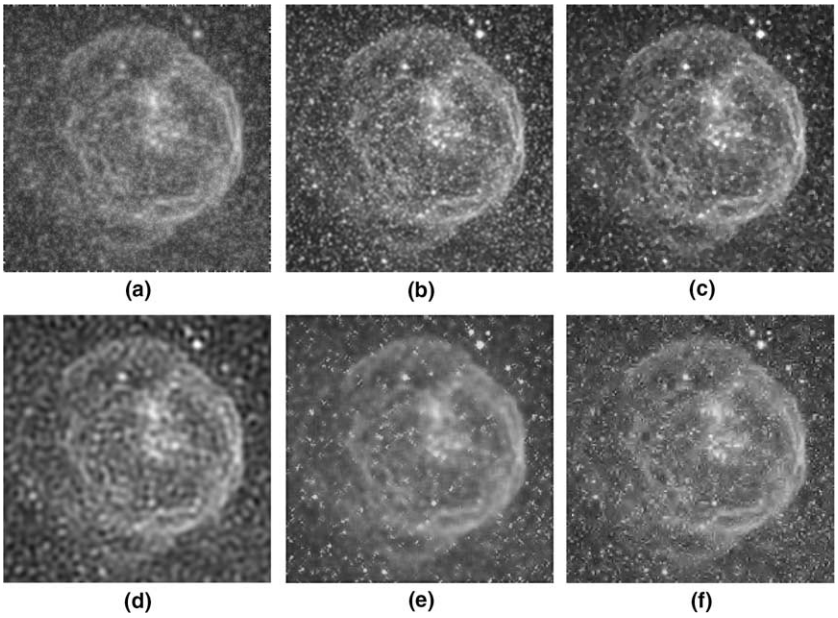

Fig. 13. Comparison of the restoration results in Fig. 1 from various filtering methods: (a) the proposed diffusion model; (b) Gaussian smoothing; (c) median filter; (d) Fourier transform; (e) Wiener filtering; (f) wavelet shrinkage.

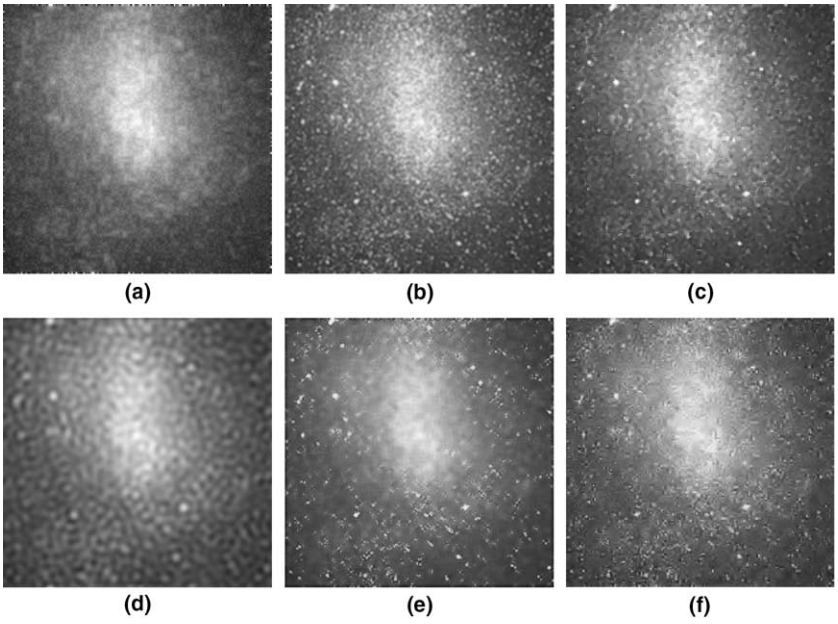

Fig. 14. Comparison of the restoration results in Fig. 10(a3) from various filtering methods: (a) the proposed diffusion model; (b) Gaussian smoothing; (c) median filter; (d) Fourier transform; (e) Wiener filtering; (f) wavelet shrinkage.

tering (Lim, 1990) and a wavelet-based bivariate shrinkage (Sendur and Selesnick, 2002). The Wiener filtering evaluated in this paper uses local mean and local variance information to filter out noise (MATLAB, 2004). The Wiener filtering method performs little smoothing when the local variance is small, and does the opposite when the variance is large. The bivariate shrinkage function uses locally adaptive estimated variances in the wavelet domain to estimate the original image. Figs. 11(e)–14(e) and 11(f)–14(f) show the restored images from the Wiener filtering and the wavelet-based bivariate shrinkage method (wavelet shrinkage), respectively. It can be observed from the figures that some larger bright stars are retained in the filtered images for both adaptive denoising methods. The results reveal that solely considering the local variance cannot effectively eliminate noisy stars. The commonly used smoothing methods and the two locally adaptive denoising methods evaluated in the experiments either fail to remove noisy stars of large size or blur the details of a nebula. The results indicate that the proposed diffusion method that considers both gradient

and variance of gray levels is well suited for the restoration of a nebula in an astronomical image.

4. Conclusions

In this paper we have proposed a modified anisotropic diffusion scheme for astronomical image restoration. The astronomical images targeted in this study are unclear nebulae obscured by stars. The noisy stars in a nebula image have different sizes and brightness, and are spread randomly. Because a large number of stars obscure the nebula all over the image, astronomers cannot easily observe the outline of the nebula. In order to restore the original appearance of a nebula, the stars must be filtered out and the detailed structure of the nebula must be well enhanced. The traditional P–M diffusion model only considers the gradient information of gray levels and, therefore, cannot effectively eliminate the noisy stars. Since the stars have higher intensities in the dark space, the stars involve higher variance of gray levels in the image. The proposed diffusion method incorporates the variance information of gray levels into the traditional diffusion coefficient function to filter out noisy stars in the image. Experimental results have shown that the proposed anisotropic diffusion scheme can effectively remove noisy stars, and yet maintain sharp edges of a nebula in the astronomical image. It can help the astronomers observe the nebula more easily from the restored image. It is believed that the proposed method can be extended for removal of impulse noise in general, and it is currently under investigation.

References

Alvarez, L., Lions, P.L., Morel, J.M., 1992. Image selective smoothing and edge detection by nonlinear diffusion. SIAM J. Numer. Anal. Arch. 29, 845–866.

Bakalexis, S.A., Boutalis, Y.S., Mertzios, B.G., 2002. Edge detection and image segmentation based on nonlinear anisotropic diffusion. In: IEEE Internat. Conf. on Digital Signal Processing 2, Santorini, Greece. pp. 1203–1206.

Barash, D., 2002. A fundamental relationship between bilateral filtering, adaptive smoothing, and the nonlinear diffusion equation. IEEE Trans. Pattern Anal. Machine Intell. 24, 844–847.

Bratsolis, E., Sigelle, M., 2003. Fast SAR image restoration, segmentation, and detection of high-reflectance regions. IEEE Trans. Geosci. Remote Sens. 41, 2890–2899.

Bretschneider, T., 2002. On the deconvolution of satellite imagery. In: IEEE Internat. Geoscience and Remote Sensing Symp., vol. 4, Toronto, Canada, pp. 2450–2452.

Chen, Y., Barcelos, C.A.Z., 2001. Smoothing and edge detection by time-varying coupled nonlinear diffusion equations. Computer Vision and Image Understanding 82, 85–100.

Deng, G., 2004. EM algorithms for robust signal filtering and prediction. In: European Signal Processing Conf., Vienna, Austria.

Deng, H., Liu, J., 2000. Unsupervised segmentation of textured images using anisotropic diffusion with annealing function. In: Internat. Symp. on Multimedia Information Processing. University of Sydney, Australia, pp. 62–67.

Dias, J.M.B., Leitao, J.M.N., 2002. The ZπM algorithm: A method for interferometric image reconstruction in SAR/SAS. IEEE Trans. Image Process. 11, 408–422.

Hamza, A.B., Krim, H., Unal, G.B., 2002. Unifying probabilistic and variational estimation. IEEE Signal Process. Mag. 19, 37–47.

Jalobeanu, A., Blanc-Feraud, L., Zerubia, J., 2000. Satellite image deconvolution using complex wavelet packets. In: Internat. Conf. on Image Processing, vol. 3, Vancouver, BC, Canada. pp. 809–812.

Lee, K.J., Papadakis, N.G., Barber, D.C., Wilkinson, I.D., Griffiths, P.D., Paley, M.N.J., 2004. A method of generalized projections (MGP) ghost correction algorithm for interleaved EPI. IEEE Trans. Medical Imaging 23, 839–848.

Lim, J.S., 1990. Two-Dimensional Signal and Image Processing. Prentice Hall, Englewood Cliffs, NJ, pp. 536–540.

MATLAB, 2004. Image Processing Toolbox User's Guide. The Math Works, Natick, MA. pp. 10–52.

Mihcak, M.K., Kozintsev, I., Ramchandran, K., Moulin, P., 1999. Low-complexity image denoising based on statistical modeling of wavelet coefficients. IEEE Signal Process. Lett. 6, 300–303.

Molina, R., 1994. On the hierarchical Bayesian approach to image restoration: Applications to astronomical images. IEEE Trans. Pattern Anal. Machine Intell. 6, 1122–1128.

Molina, R., Nunez, J., Cortijo, F.J., Mateos, J., 2001. Image restoration in astronomy: A Bayesian perspective. IEEE Signal Process. Mag. 18, 11–29.

Moulin, P., Liu, J., 1999. Analysis of multiresolution image denoising schemes using generalized Gaussian and complexity priors. IEEE Trans. Inform. Theory 45, 909–919.

Niessen, W.J., Vincken, K.L., Weickert, J.A., Viergever, M.A., 1997. Nonlinear multiscale representations for image segmentation. Computer Vision and Image Understanding 66, 233–245.

Nikolova, M., 1999. Markovian reconstruction using a GNC approach. IEEE Trans. Image Process. 8, 1204–1220.

Perona, P., Malik, J., 1990. Scale-space and edge detection using anisotropic diffusion. IEEE Trans. Pattern Anal. Machine Intell. 12, 629–639.

Rathee, S., Koles, Z.J., Overton, T.R., 1992. Image restoration in computed tomography: Restoration of experimental CT images. IEEE Trans. Med. Imaging 11, 546–553.

Sapiro, G., Ringach, D.L., 1996. Anisotropic diffusion of multivalued images with applications to color filtering. IEEE Trans. Image Process. 5, 1582–1586.

Sendur, L., Selesnick, I.W., 2002. Bivariate shrinkage with local variance estimation. IEEE Trans. Signal Process. Lett. 9, 438–441.

Solé, A.F., López, A., 2001. Crease enhancement diffusion. Computer Vision and Image Understanding 84, 241–248.

Starck, J.L., Pantin, E., Murtagh, F., 2002. Deconvolution in astronomy: A review. Astron. Soc. Pacific 114, 1051–1069.

Starck, J.L., Candes, E., Donoho, D.L., 2003. Astronomical image representation by the curvelet transform. Astron. Astrophys. 398, 785–800.

Torkamani-Azar, F., Tait, K.E., 1996. Image recovery using the anisotropic diffusion equation. IEEE Trans. Image Process. 5, 1573–1578.

Tsai, D.-M., Chao, S.-M., 2005. An anisotropic diffusion-based defect detection for sputtered surfaces with inhomogeneous textures. Image and Vision Computing 23, 325–338.

Tsuji, H., Sakatani, T., Yashima, Y., Kobayashi, N., 2002. A nonlinear spatio-temporal diffusion and its application to prefiltering in MPEG-4 video coding. In: Proc. Internat. Conf. on Image Processing I, Rochester, New York. pp. 85–88.

Wen, C.-Y., Lee, C.-H., 2002. Point spread functions and their applications to forensic image restoration. Forensic Sci. J. 1, 15–26.

Wu, H.-S., Barba, J., 1998. Minimum entropy restoration of star field images. IEEE Trans. Systems Man Cybernet.: Part B 28, 227–231.

You, Y.-L., Kaveh, M., 1999. Blind image restoration by anisotropic regularization. IEEE Trans. Image Process. 8, 396–407.

You, Y.-L., Xu, W., Tannenbaum, A., Kaveh, M., 1996. Behavioral analysis of anisotropic diffusion in image processing. IEEE Trans. Image Process. 5, 1539–1553.